BOLETIN DE LA SOCIEDAD ESPAÑOLA DE
Cerámica y Vidrio
A R T I C U L O

Synthesis and characterization of sodium cation-conducting $Na_x(M_yL_{1-y})O_2$ ($M = Ni^{2+}, Fe^{3+}$; $L = Ti^{4+}, Sb^{5+}$)

O.A. SMIRNOVA[A], V.V. KHARTON[A,B], F.M.B. MARQUES[A]

[a] Department of Ceramics and Glass Engineering, CICECO, University of Aveiro, 3810-193 Aveiro, Portugal
[b] Institute of Physicochemical Problems, Belarus State University, 14 Leningradskaya Str., 220050 Minsk, Belarus

The Na^+-conducting ceramics of layered $Na_{0.8}Ni_{0.4}Ti_{0.6}O_2$, $Na_{0.8}Fe_{0.8}Ti_{0.2}O_2$, $Na_{0.8}Ni_{0.6}Sb_{0.4}O_2$ (structural type O3) and $Na_{0.68}Ni_{0.34}Ti_{0.66}O_2$ (P2 type) with density higher than 91% were prepared via the standard solid-state synthesis route and characterized by the impedance spectroscopy, thermal analysis, scanning electron microscopy, structure refinement using X-ray powder diffraction data, measurements of Na^+ concentration cell e.m.f., and dilatometry. The conductivity of antimonate $Na_{0.8}Ni_{0.6}Sb_{0.4}O_2$, synthesized first time, was found lower than that of isostructural $Na_{0.8}Ni_{0.4}Ti_{0.6}O_2$ due to larger ion jump distance between Na^+ sites. At temperatures above 420 K, transport properties of sodium cation-conducting materials are essentially independent of partial water vapor pressure. In the low-temperature range, the conductivity reversibly increases with water vapor pressure varied in the range from approximately 0 (dry air) up to 0.46 atm. The sensitivity to air humidity is influenced by the ceramic microstructure, being favored by increasing boundary area. The average thermal expansion coefficients of layered materials at 300-1173 K are in the range $(13.7\text{-}16.0)\times10^{-6}$ K^{-1}.

Keywords: sodium cationic conductor, impedance spectroscopy, air humidity, thermal expansion, ceramic microstructure

Síntesis y caracterización del conductor catiónico de sodio $Na_x(M_yL_{1-y})O_2$ ($M = Ni^{2+}, Fe^{3+}$; $L = Ti^{4+}, Sb^{5+}$)

Se han preparado cerámicas conductoras conteniendo Na^+ de composición $Na_{0.8}Ni_{0.4}Ti_{0.6}O_2$, $Na_{0.8}Fe_{0.8}Ti_{0.2}O_2$, $Na_{0.8}Ni_{0.6}Sb_{0.4}O_2$ (tipo estructural O3) y $Na_{0.68}Ni_{0.34}Ti_{0.66}O_2$ (tipo P2) con densidad mayor del 91%. Las vía de preparación fu la ruta de estandard de síntesis en estado sólido. Las composiciones se caracterizaron mediante espectroscopía de impedancia, análisis térmico, microscopía electrónica de barrido, refinamiento de la estructura usando datos de difracción de rayos X en polvo, medidas de concentración de Na^+, f.e.m. de la célula y dilatometría. La conductividad del antimoniate, sintetizado por primera vez, $Na_{0.8}Ni_{0.6}Sb_{0.4}O_2$, era menor que la del compuesto isoestructural $Na_{0.8}Ni_{0.4}Ti_{0.6}O_2$ debido a la mayor distancia de salto iónico entre las posiciones de Na^+. A temperaturas por encima de 420 K, las propiedades de transporte de los materiales conductores que contienen cations sodio son esencialmente independientes de la presión parcial de vapor de agua. En el intervalo de baja temperatura, la conductividad aumenta reversiblemente con la presión de vapor de agua variando en un intervalo de aproximadamente 0 (aire seco) hasta 0.46 atm. La sensibilidad a la humedad del aire está influída por la microestructura de la cerámica, estando favorecida al aumentar el área de borde. Los coeficientes de dilatación térmica medios de los materiales laminares entre 300 y 1173 K están en el intervalo $(13.7\text{-}16.0)\times10^{-6}$ K^{-1}.

Palabras clave: conductor con cationes sodio, espectroscopia de impedancia, humedad del aire, dilatación térmica, microestructura cerámica.

1. INTRODUCTION

Solid-state alkali-cation conductors are receiving a great attention for applications in rechargeable batteries [1], ion selective electrodes [2], gas sensors [3,4]. Fast alkali cation transport requires a lattice with favorable diffusion pathways, i.e. the metal-oxygen polyhedra occupied by charge carriers should be connected in one (tunnel structures), two (layered structures) or, most preferable, three dimensions forming a pathway through the unit cell. One of the best groups of sodium ion conductors, so-called NASICONs, is characterized by a three-dimensional conductivity path [5]; β-alumina has a layered structure [6]. Another family of layered compounds, having cationic conductivity comparable to those of NASICONs, comprises several structural types based on brucite-like octahedral layers $MO_{6/3}$ (where M is transition metal) sandwiching alkali cations between them [7-11]. According to the nomenclature developed for these phases by Hagenmuller et al. [7] known structures are separated into P3, O3, P2, O2, O6 and T2 types. In this notation the letter indicates the coordination of an interlayer alkali cation (**O**ctahedral, trigonal **P**rismatic or **T**etrahedral) and the digit corresponds to the number of layers in the unit cell. Such crystal lattices usually have a lot of free space between $MO_{6/3}$ layers where water can be intercalated to solvate alkali cations [12]. Various applications of Na^+ ionic conductors require maximum stability, including possible minimum reactivity with water vapor. On the other hand, materials showing a significant and reversible response to the humidity variations are of importance for sensors construction.

This work was centered on the comparative studies of several layered phases (O3 and P2 types), in particular on the evaluation of their behavior in H_2O-containing atmospheres. In order to assess possible interaction mechanisms with water vapor, the results of impedance spectroscopy, differential thermal and thermogravimetric analysis (DTA/TGA) and X-ray diffraction (XRD) are used. One particular goal was to determine thermal expansion of Na^+-conducting ceramics. The values of thermal expansion coefficients (TECs) determine compatibility with other materials at elevated temperatures, and thus are among key properties of a solid electrolyte considered for practical applications.

2. EXPERIMENTAL

Dense ceramic samples of $Na_{0.8}Ni_{0.4}Ti_{0.6}O_2$, $Na_{0.8}Fe_{0.8}Ti_{0.2}O_2$, $Na_{0.8}Ni_{0.6}Sb_{0.4}O_2$ (O3-type) and $Na_{0.68}Ni_{0.34}Ti_{0.66}O_2$ (P2) were prepared by a standard solid-state reaction technique from $Na_2CO_3{\cdot}10H_2O$ (Merck), $Ni(NO_3)_2{\cdot}6H_2O$ (Aldrich), Fe_2O_3 (Merck), TiO_2 (Merck), and Sb_2O_5 (Aldrich). The appropriate amounts of the reagents were ball-milled with ethanol, dried and calcined in several stages with intermediate millings to obtain almost single-phase powders. The powders were pressed uniaxially and then isostatically at 200 MPa into disks (diameter 1.0-1.8 cm), and sintered in packing powder of the same composition in closed alumina containers in order to prevent sodium losses. Table I represents the sintering conditions for all of the compositions. The color of the ceramic specimens was brown for $Na_{0.8}Fe_{0.8}Ti_{0.2}O_2$, light-green for $Na_{0.8}Ni_{0.6}Sb_{0.4}O_2$ and green for $Na_{0.8}Ni_{0.4}Ti_{0.6}O_2$ and dark-green for $Na_{0.68}Ni_{0.34}Ti_{0.66}O_2$. Note that, in order to avoid Na_2O volatilization, the temperature and the time of sintering were chosen minimum necessary to obtain homogeneous dense ceramics. Density values were calculated from the geometry and weight of the bulk ceramic specimens and expressed as a percentage of the theoretical density calculated from the structural data (Table I).

TABLE I. SINTERING CONDITIONS AND PHYSICOCHEMICAL PROPERTIES OF CERAMIC MATERIALS

Composition	Sintering	ρ, g/cm³	ρ, %	σ(mS/cm) 573 K, dry air	E_a (kJ/mol) dry air	$\sigma_{wet}/\sigma_{dry}$ * 373 K	TEC $\alpha\times10^6$, K⁻¹ 300-1173 K
$Na_{0.68}Ni_{0.34}Ti_{0.66}O_2$	1373 K, 3h	3.65	94	97.0	32	1.2	15.70±0.06
$Na_{0.8}Ni_{0.4}Ti_{0.6}O_2$	1298 K, 3h	3.69	91	10.9	37	1.2	14.79±0.09
$Na_{0.8}Fe_{0.8}Ti_{0.2}O_2$	1123 K, 3h	3.76	92	20.5	33	1.7	16.0±0.4
$Na_{0.8}Ni_{0.6}Sb_{0.4}O_2$	1543 K, 3h	4.62	91	3.20	48	1.26	13.66±0.06

* Note: σ_{wet} corresponds to $p(H_2O)$=0.46 atm

Phase purity of the ceramic materials was verified by XRD (Rigaku D/Max-B diffractometer, CuK_α radiation, graphite monochromator). FullProf software [13] was used to refine the crystal structures; the unit cell parameters in the case of hydrated phases were calculated using Checkcell program. The ceramic microstructure was studied by scanning electron microscopy (SEM) using a Hitachi S4100 instrument; the samples for SEM examination were polished and thermally etched for 0.5 h at temperatures 100-200 K lower than the sintering temperature. Thermal expansion was measured using an alumina Linseis dilatometer at 300-1173 K in air at heating rate of 5°/min. Impedance spectroscopy measurements were performed with a Hewlett Packard 4284A LCR meter (frequency range from 20 Hz up to 1 MHz) in a flow of dry air, dry argon and humidified air where the water vapor partial pressure, $p(H_2O)$, varied from approximately 0 up to 0.46 atm. Wet air was obtained by bubbling through deionized water; the humidity level was controlled by the water temperature with an accuracy of 1 K. For each measurement, the samples were kept in flowing humidified air up to 24 hours to achieve time-independent conductivity values. SETARAM TG-DTA LabSys instrument was used for thermogravimetric and differential thermal analysis (TG/DTA) studies. The evaluation of ionic transference numbers by electromotive force technique was performed at room temperature using Na^+,Pt | $Na_{0.68}Ni_{0.34}Ti_{0.66}O_2$ | Pt,Na^+ cells where the sodium activity at the electrodes was determined by $(CH_3COO)Na$ concentration in ethanol solutions.

3. RESULTS AND DISCUSSION

3.1. Structure and microstructure

For $Na_{0.68}Ni_{0.34}Ti_{0.66}O_2$ (P2-type), $Na_{0.8}Ni_{0.4}Ti_{0.6}O_2$ (O3) and new mixed nickel-sodium antimonate $Na_{0.8}Ni_{0.6}Sb_{0.4}O_2$ (O3), the optimized sintering conditions listed in Table I made it possible to prepare single-phase ceramics with density higher than 91%. $Na_{0.8}Fe_{0.8}Ti_{0.2}O_2$ (O3) ceramics are characterized by trace amounts of β-$NaFeO_2$ detected by XRD. Increasing sintering temperature could not suppress the formation of this phase; the processing conditions of $Na_{0.8}Fe_{0.8}Ti_{0.2}O_2$ were thus selected in order to simultaneously obtain minimum secondary phase concentration (~3%) and maximum density (~92%). As a particular result, SEM micrographs of $Na_{0.8}Fe_{0.8}Ti_{0.2}O_2$ ceramics show small grains of irregular shape, while other phases have platelet grains characteristic of layered hexagonal structure (Fig.1). The increase of the sintering temperature leads to larger grain size of Ti-containing materials. On the contrary, Sb-containing ceramics sintered at quite high temperature (Table I) are characterized by a relatively small grain size and less glassy phase at the boundaries. Closed pores were observed in the case of $Na_{0.68}Ni_{0.34}Ti_{0.66}O_2$ and, to a lower extent, in the case of $Na_{0.8}Fe_{0.8}Ti_{0.2}O_2$.

Table II represents XRD data collection conditions and Rietveld refinement results; selected examples of the observed and calculated diffraction patterns are shown in Fig.2. The structural data obtained for nickel-sodium titanates $Na_{0.68}Ni_{0.34}Ti_{0.66}O_2$ (P2) and $Na_{0.8}Ni_{0.4}Ti_{0.6}O_2$ (O3) are in good agreement with those reported in literature [14]. The new mixed nickel-sodium antimonate, $Na_{0.8}Ni_{0.6}Sb_{0.4}O_2$, was found to crystallize in the same structural type as $Na_{0.8}Ni_{0.4}Ti_{0.6}O_2$. In the structural family under consideration, the cell parameter **a** is equal to the edge of MO_6 (M = Ni^{2+}, Fe^{3+}, Ti^{4+}, Sb^{5+}) octahedra. Average radius of M cations, randomly placed in octahedral sites, increases in the sequence $Na_{0.68}Ni_{0.34}Ti_{0.66}O_2$ (0.774 Å) > $Na_{0.8}Ni_{0.4}Ti_{0.6}O_2$ (0.779 Å) > $Na_{0.8}Ni_{0.6}Sb_{0.4}O_2$ (0.794 Å) leading therefore to increasing **a** parameter. $Na_{0.8}Fe_{0.8}Ti_{0.2}O_2$ is characterized by a slightly lower average M radius (0.777 Å), but slightly larger **a** parameter as compared to $Na_{0.8}Ni_{0.4}Ti_{0.6}O_2$, obviously due to higher ionicity of M-O bonds in the iron-sodium titanate structure. The parameter **c** is determined by the interlayer distance and strongly depends on the amount of sodium ions placed between $MO_{6/3}$ octahedral layers. Decreasing sodium content results in a higher repulsion of oxygen anions, therefore the interlayer distance in $Na_{0.68}Ni_{0.34}Ti_{0.66}O_2$ lattice is larger than that of other layered phases.

TABLE II. STRUCTURAL PROPERTIES, XRD DATA COLLECTION AND RIETVELD REFINEMENT DETAILS

Composition	$Na_{0.68}Ni_{0.34}Ti_{0.66}O_2$	$Na_{0.8}Ni_{0.4}Ti_{0.6}O_2$	$Na_{0.8}Fe_{0.8}Ti_{0.2}O_2$	$Na_{0.8}Ni_{0.6}Sb_{0.4}O_2$
Structure type	P2	O3	O3	O3
Crystal system:	trigonal	trigonal	trigonal	trigonal
Space group:	$P6_3/mmc$ (no. 166)	R-3m (no. 166)	R-3m (no. 166)	R-3m (no. 166)
Unit cell dimensions (Å, degrees)	a = 2.96226(8) b = 11.1496(4)	a = 2.983(1) b = 16.374(5)	a = 3.0019(1) b = 16.3677(9)	a = 3.04820(7) b = 16.3993(5)
Cell volume (Å³)	84.73	126.18	127.75	131.97
Z (formula units per cell)	2	3	3	3
Theoretical density (g/cm³)	3.887	4.059	4.089	5.078
2θ range (°)	10 – 130	10 – 130	10 – 130	10 – 130
Number of data points	6000	6000	6000	6000
Number of reflections	48	45	44	46
Number of parameters	21	20	19	19
Agreement factors:				
R_p, %	9.37	7.44	14.4	8.33
R_{wp}, %	12.7	9.53	19.4	10.8
R_{exp}, %	7.07	7.19	10.78	4.91
χ^2	3.21	1.76	3.25	4.81

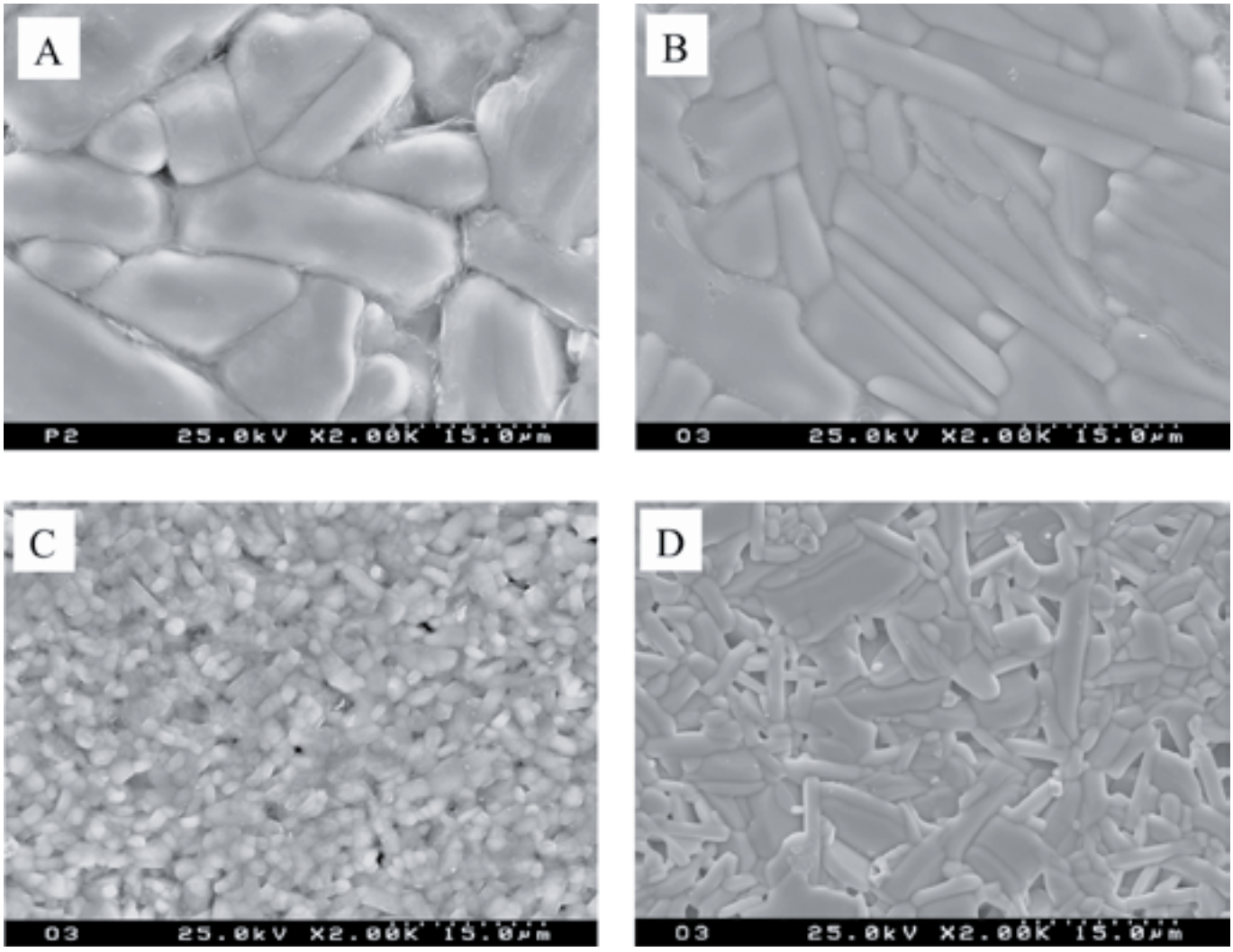

Fig.1. SEM micrographs of Na^+-conducting layered ceramic materials: A – $Na_{0.68}Ni_{0.34}Ti_{0.66}O_2$, B – $Na_{0.8}Ni_{0.4}Ti_{0.6}O_2$, C - $Na_{0.8}Fe_{0.8}Ti_{0.2}O_2$, D - $Na_{0.8}Ni_{0.6}Sb_{0.4}O_2$

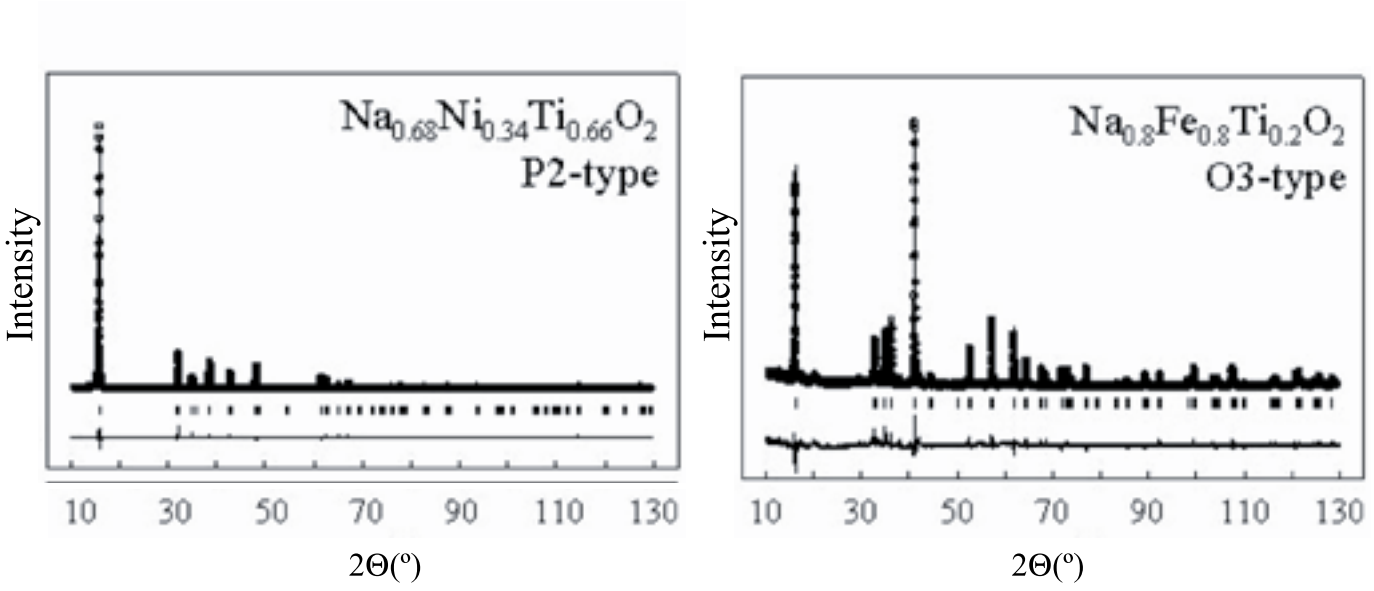

Fig.2. Final observed, calculated and difference XRD patterns of the compounds with P2- and O3-type structure.

3.2. Thermal expansion

Dilatometric studies showed that thermal expansion at 300-1173 K can be described with a standard linear model for all studied materials (Fig.3). For Ni-containing compounds, increasing of nickel cation concentration in the octahedral layers from 34 to 60% is accompanied with decreasing average thermal expansion coefficients (TECs) from 15.7×10^{-6} to 13.7×10^{-6} K^{-1}. $Na_{0.8}Fe_{0.8}Ti_{0.2}O_2$ is characterized by the higher TEC value, 16.0×10^{-6} K^{-1}. These variations in thermal expansion coefficients, as well as the absolute TEC values are quite similar to those of Ni- and Fe-containing perovskite oxides [15].

The isostructural O3-type compounds $Na_{0.8}Ni_{0.6}Sb_{0.4}O_2$, $Na_{0.8}Fe_{0.8}Ti_{0.2}O_2$ and $Na_{0.8}Ni_{0.4}Ti_{0.6}O_2$ show a linear correlation between the conductivity and TECs (Fig.3), as observed for oxygen ion-conducting solid electrolytes [16]. The phenomenological theory of ionic transport [17] qualitatively explains this behavior by the increasing mobility of ionic defects with thermal expansion of the crystal.

3.3. Conductivity in dry atmospheres

Fig.4 represents the temperature dependencies of total conductivity (σ) determined from the impedance spectra in various atmospheres. As expected, changes of the oxygen partial pressure, at least in the range from 0.21 atm (dry air) to 1×10^{-5} atm (dry argon), do not affect the conductivity. Thus the variations in σ values due to changes in the water vapor partial pressure, discussed below, cannot be attributed to variations in the electronic transport resulting from oxygen losses or incorporation into the lattice. Indeed, at temperatures below 700 K, the ion transference numbers (t_{ion}), evaluated by e.m.f. measurements in Na^+ concentration cells and using Hebb-Wagner technique, are higher than 0.99. Table III lists the values of t_{ion}, measured by the modified e.m.f. technique taking electrode polarization into account [18], for $Na_{0.68}Ni_{0.34}Ti_{0.66}O_2$ phase. The electron transference numbers are

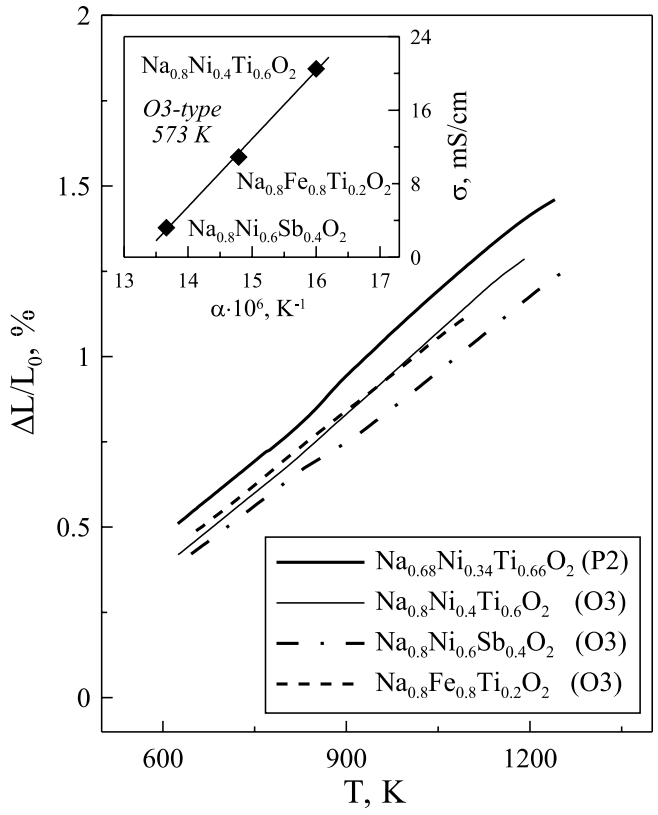

Fig.3. Dilatometric curves of Na^+-conducting ceramics. Inset shows TEC-conductivity relationship for layered materials with O3-type structure.

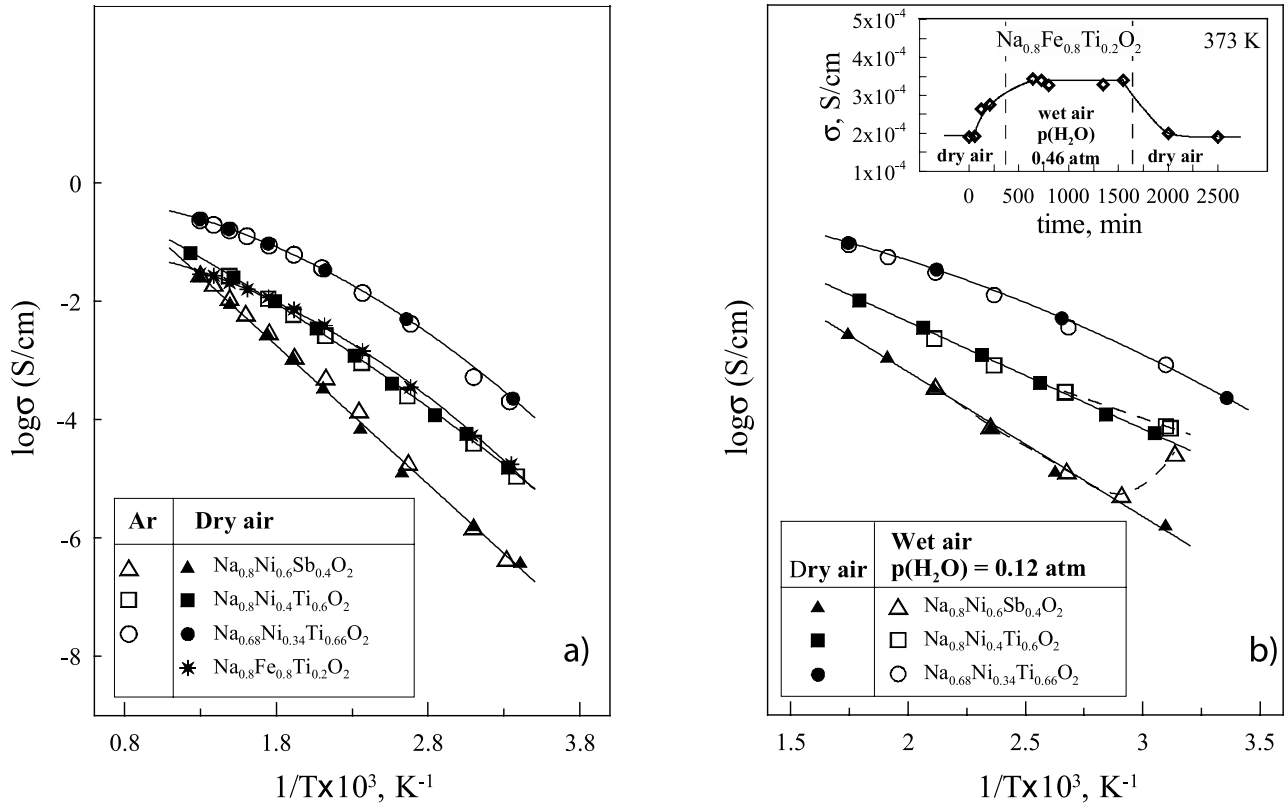

Fig.4. Temperature dependence of total conductivity of the studied materials in dry air, dry argon (left) and wet air (right). Inset shows time dependence of the conductivity of $Na_{0.8}Fe_{0.8}Ti_{0.2}O_2$ ceramics after $p(H_2O)$ variations, showing reversibility and approximate relaxation time (top right)

lower than 0.0005 although a significant electronic contribution to the total conductivity might be expected due to the presence of variable-valence nickel cations in the lattice. These values are even lower than the measurement error of the e.m.f. technique, thus ensuring that at low temperatures $Na_{0.68}Ni_{0.34}Ti_{0.66}O_2$ is a Na^+ cation-conducting solid electrolyte. Similar results were obtained for all studied materials; detailed data on their electronic conductivity will be published elsewhere. In general, electronic transport in the studied sodium cation conductors can be neglected when analyzing σ vs. $p(H_2O)$ dependence.

TABLE III. SODIUM CATION TRANSFERENCE NUMBERS OF $NA_{0.68}NI_{0.34}TI_{0.66}O_2$ MEASURED BY MODIFIED E.M.F. TECHNIQUE AT 298 K USING ETHANOL SOLUTIONS WITH DIFFERENT NA^+ ACTIVITIES

Na^+ concentration gradient	T_{ion}
0.1 / 0.01 M	0.9999
0.1 / 0.002 M	0.9996
0.1 / 0.0001 M	0.9996

Among layered phases, the structures with prismatic coordination of sodium show typically a higher conductivity compared to octahedral [9,11]. In P2-type structure, sodium ions are distributed within a layer of equivalent prisms with wide square bottlenecks. This results in a considerably higher sodium mobility than that in O3-type lattice comprising octahedral sodium hosts, small tetrahedrally-coordinated interstitial positions and triangle bottlenecks between them. Another reason for higher conductivity values is higher sodium deficiency in P2-type compounds, which usually have lower x values according to the general formula $Na_xM_{x/2}Ti_{1-x/2}O_2$ (M = Ni, Co) [9,11]. Therefore, P2-type $Na_{0.68}Ni_{0.34}Ti_{0.66}O_2$ shows maximum conductivity with respect to other studied materials. To compare the conductivity of isostructural O3-type phases characterized by equal sodium vacancy concentration, several features as ionicity of M-O framework, bottleneck size and jump distance between sodium sites, equal to the **a** parameter (Table II), must be considered. In the sequence $Na_{0.8}Ni_{0.4}Ti_{0.6}O_2$ - $Na_{0.8}Fe_{0.8}Ti_{0.2}O_2$ - $Na_{0.8}Ni_{0.6}Sb_{0.4}O_2$ the bottleneck size decreases (2.13 Å – 2.06 Å – 2.04 Å), while jump distance between sodium sites increases. Finally, the conductivities of $Na_{0.8}Fe_{0.8}Ti_{0.2}O_2$ and $Na_{0.8}Ni_{0.4}Ti_{0.6}O_2$ are close to each other, which seems as a result of the sum of structural and microstructural features. $Na_{0.8}Ni_{0.6}Sb_{0.4}O_2$ has almost the same bottleneck size as $Na_{0.8}Fe_{0.8}Ti_{0.2}O_2$, but exhibits the lowest conductivity due to the high activation energy, likely related to because of the highest sodium jump distance. Considering the character of conductivity temperature dependencies, one should also point out the anomalously high preexponential term characteristic of the antimony-containing phase. The value is even higher than that of P2-type compound, where the ratio between sodium and empty site concentrations is most favorable. This fact can be explained by the higher electronegativity of antimony and consequent lower ionicity of (Ni, Sb) – O framework mentioned above, leading to the weaker Na-O bonds.

Also one should note the important role of ceramic microstructure. The conductivity of studied layered titanates (Fig.4) is substantially higher than the values reported for similar ceramic materials, $Na_{0.8}Fe_{0.8}Ti_{0.2}O_2$ [10] and $Na_xNi_{x/2}Ti_{1-x/2}O_2$ [9,11]. The most probable reason is the higher density achieved in this work. Furthermore, selected ceramics exhibit activation energy changes with temperature, which also seems due to the microstructure. As it was demonstrated for sodium rare-earth silicates [19], with increasing temperature, the conductivity of partly blocking grain boundaries contributes less to the total conductivity, thus decreasing the activation energy. In the present work, an activation energy decrease with temperature is registered for $Na_{0.8}Fe_{0.8}Ti_{0.2}O_2$, characterized by the smallest grain size, and also for $Na_{0.68}Ni_{0.34}Ti_{0.66}O_2$, the latter showing a large amount of glassy phase along the grain boundaries.

3.4. Conductivity in H_2O-containing atmospheres

At temperatures below 450 K, the presence of water vapor in the atmosphere results in higher σ values as illustrated by Fig.4. The initial values of the conductivity can be reproduced after experiments with an accuracy of 3-5%, comparable to the conductivity measurement error (Fig.4), i.e. the observed changes are completely reversible. In order to investigate possible mechanisms of interaction with water vapor, a series of ceramic samples was kept in wet air at 373 K and $p(H_2O)$=0.46 atm for 24 hours, ground into powders and then studied by XRD and TG/DTA. The exposition time was estimated from the conductivity relaxation data to achieve equilibrium with water vapor (Fig.4).

As mentioned above, the layered phases can easily absorb water between $MO_{6/3}$ layers sandwiching sodium cations. Hence an increase in the interlayer distance and, thus, lattice parameter **c** due to water incorporation can be expected. Indeed, for $Na_{0.8}Ni_{0.4}Ti_{0.6}O_2$ and $Na_{0.8}Ni_{0.6}Sb_{0.4}O_2$ samples after treatment in water vapor, XRD patterns show an appearance of hydrated phases having larger **c** and essentially the same **a** parameter, compared to initial phases. In Fig.5, the reflections of hydrated phases are marked with subscript "aq"; as expected, the (003) and (006) reflections are strongly shifted to lower 2θ region. The **c** parameters were calculated from 7-10 reflections with high l-contribution (003, 006, 009, 018 etc.). These parameters

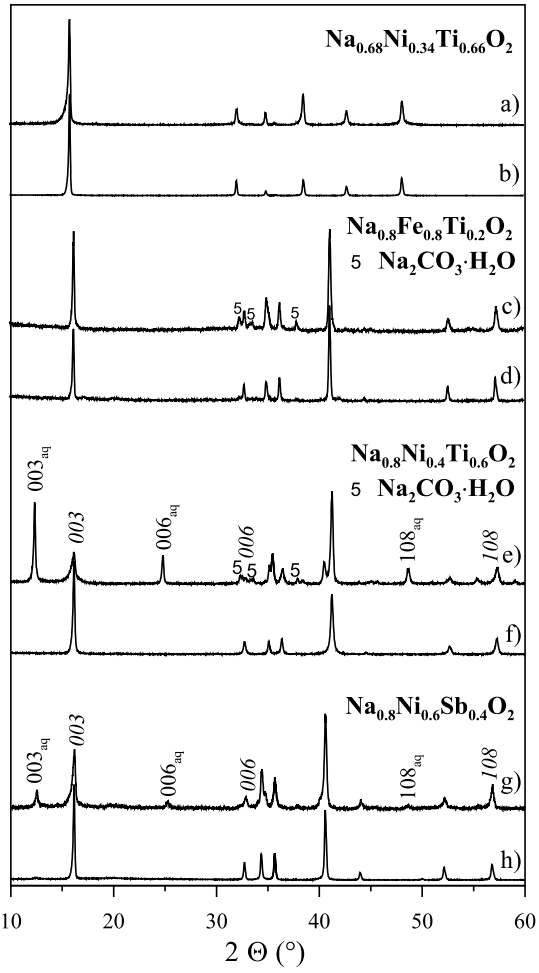

Fig.5.. Comparison of the XRD patterns of layered phases after hydration (a, c, e, g) and after annealing (b, d, f, h). Dense ceramics were exposed to humid air at 373 K and $p(H_2O)$=0.46 atm for 24 hours. Triangles indicate peaks of $Na_2CO_3 \cdot H_2O$ phase formed due to interaction with atmospheric CO_2. Subsript "aq" indicates peaks of hydrated layered phases.

increase by approximately 30% and are equal to 21.50 Å and 21.38 Å for hydrated $Na_{0.8}Ni_{0.4}Ti_{0.6}O_2$ and $Na_{0.8}Ni_{0.6}Sb_{0.4}O_2$, respectively. The **a** parameter is 3.00 Å for both hydrated phases, i.e. remains almost unchanged. It is also important to note that the amount of hydrated phase formed in $Na_{0.8}Ni_{0.4}Ti_{0.6}O_2$ ceramics is substantially larger than that in $Na_{0.8}Ni_{0.6}Sb_{0.4}O_2$.

No evidence for grain bulk hydration or secondary phase formation was observed in the XRD patterns of P2-type $Na_{0.68}Ni_{0.34}Ti_{0.66}O_2$ (Fig.5). A similar behavior is characteristic of $Na_{0.8}Fe_{0.8}Ti_{0.2}O_2$ where no hydrated phase is formed, but the XRD pattern shows the peaks of $Na_2CO_3 \square H_2O$ marked in Fig.5 by triangles. The presence of sodium carbonate could be ascribed either to increasing sodium deficiency or to a partial ionic exchange followed by reaction with atmospheric CO_2, for example:

$$Na_{0.8}Fe_{0.8}Ti_{0.2}O_2 + (0.8x)H_2O + (0.4x)CO_2 \rightarrow (Na_{1-x}H_x)_{0.8}Fe_{0.8}Ti_{0.2}O_2 + (0.4x)Na_2CO_3 \square H_2O$$

The unit cell parameters are essentially unaffected by interaction with water, which suggests that this reaction predominantly occurs in $Na_{0.8}Fe_{0.8}Ti_{0.2}O_2$ surface layers and/or at the grain boundaries. Particularly, a part of absorbed water can be incorporated by the secondary β-$NaFeO_2$ phase. The formation of $Na_2CO_3 \square H_2O$ is also observed in the XRD patterns of $Na_{0.8}Ni_{0.4}Ti_{0.6}O_2$ (Fig. 5).

TGA analysis revealed a substantial weight loss for all hydrated materials on heating up to 373 K, which is accompanied by endothermal DTA effect and can be undoubtedly attributed to water evaporation. Notice that dehydration of $Na_2CO_3 \square H_2O$ may be expected at 370-420 K, whilst decomposition of Na_2CO_3 take place at considerably higher temperatures [19]. The water content per one sodium ion, extracted from thermogravimetric data, increases in a sequence $Na_{0.8}Ni_{0.4}Ti_{0.6}O_2 < Na_{0.8}Ni_{0.6}Sb_{0.4}O_2 < Na_{0.68}Ni_{0.34}Ti_{0.66}O_2 < Na_{0.8}Fe_{0.8}Ti_{0.2}O_2$. This seems in contradiction to XRD results, suggesting maximum stability for $Na_{0.68}Ni_{0.34}Ti_{0.66}O_2$ and, possibly, $Na_{0.8}Ni_{0.6}Sb_{0.4}O_2$ phases. One may assume that water absorption in $Na_{0.68}Ni_{0.34}Ti_{0.66}O_2$ takes place, to a considerable extent, via interaction with the glassy phase, accompanied by the formation of amorphous hydrates at the grain boundaries, which cannot be detected by XRD.

Fig. 6 presents selected examples of the impedance spectra collected in dry and wet atmospheres. In cases when bulk and grain-boundary contributions can be clearly separated (for example, Fig. 6c and 6e); one can conclude that the increase of total conductivity in wet atmospheres is mostly associated with an increase of the grain-boundary conduction. However, such a behavior could also be affected by water condensation and surface transport, especially in the case of $Na_{0.8}Ni_{0.6}Sb_{0.4}O_2$ where stepwise decrease of the boundary resistance appears at high water vapor pressures (Fig.6e). In addition, a smooth decrease in the bulk resistivity of $Na_{0.8}Ni_{0.6}Sb_{0.4}O_2$ was observed (Fig.6d). The latter phenomenon is presumably due to water intercalation between octahedral $MO_{6/3}$ layers, which can influence sodium cation transport and/or introduce protonic condictivity. Selected examples of isothermal dependencies of total conductivity vs. $p(H_2O)$ are represented in Fig. 7, usually showing S-like shape, which also supports the assumption of relevant proton conductivity. The grain-boundary conductivity response to the atmosphere humidity has a more complex nature and can be affected by

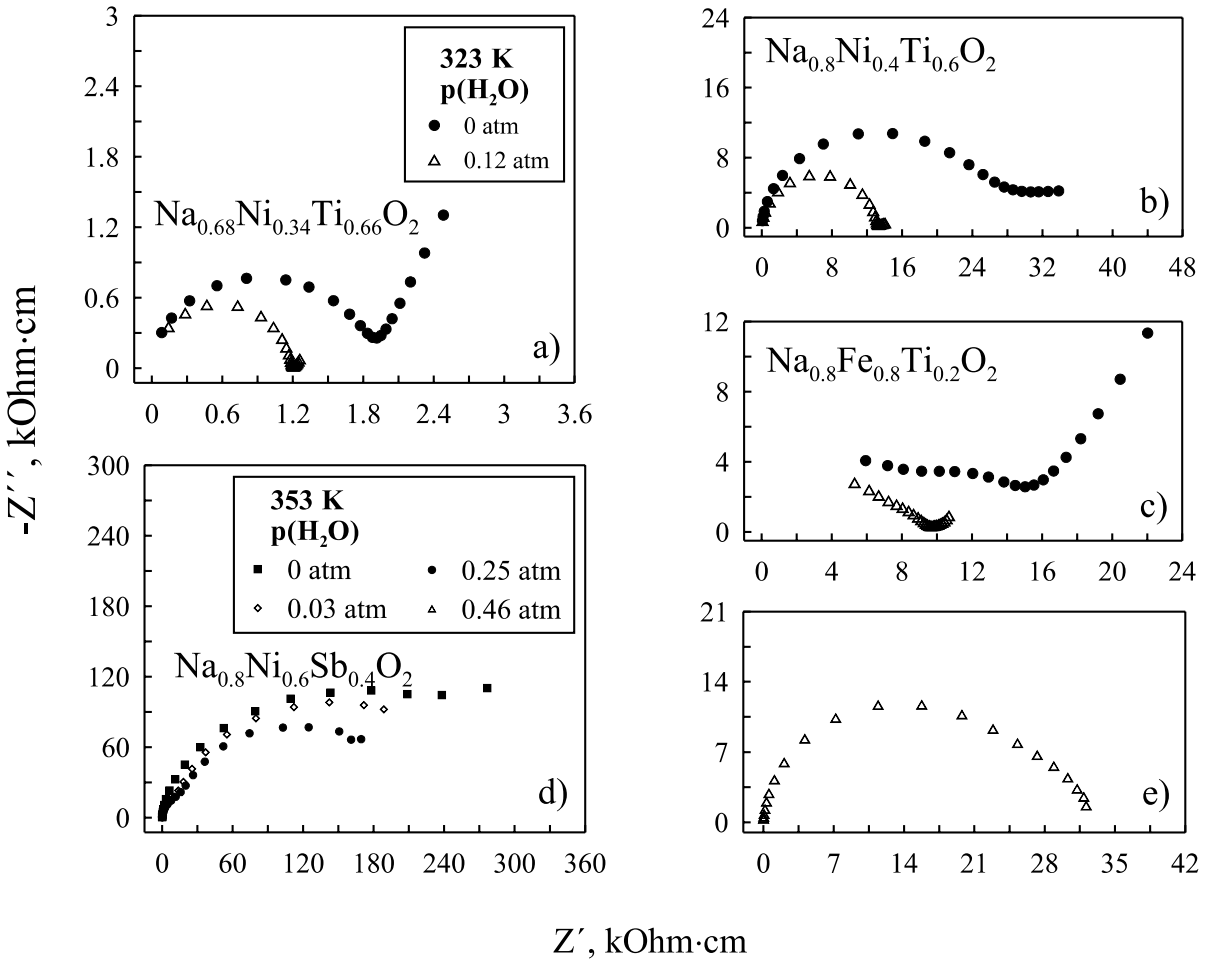

Fig.6. Typical impedance spectra of Na^+-conducting ceramics in dry and wet atmospheres.

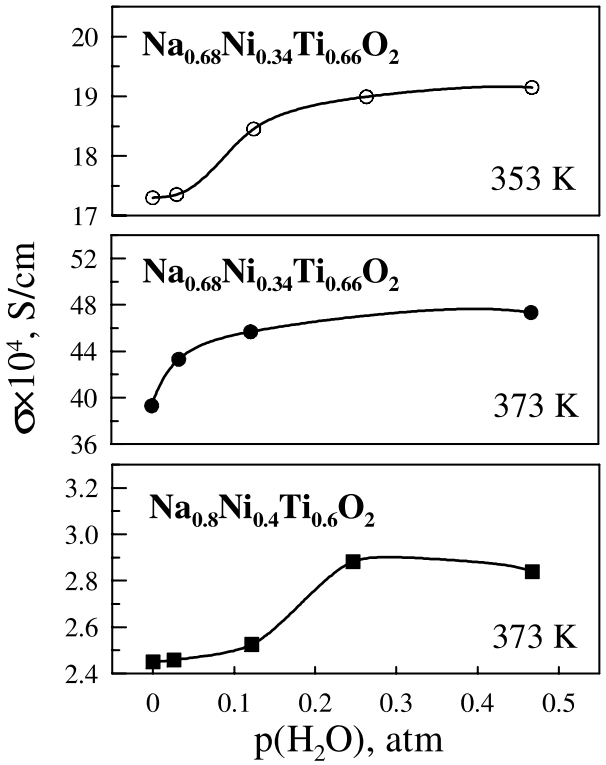

Fig.7. Isothermal dependencies of total conductivity of Na^+-conducting ceramics on the water vapor partial pressure.

numerous factors, including sodium content, porosity, grain-boundary area, and also a presence of glassy phases.

The sensitivity of total conductivity to air humidity increases in the sequence $Na_{0.8}Ni_{0.4}Ti_{0.6}O_2 < Na_{0.68}Ni_{0.34}Ti_{0.66}O_2 < Na_{0.8}Ni_{0.6}Sb_{0.4}O_2 < Na_{0.8}Fe_{0.8}Ti_{0.2}O_2$ (Table I), which correlates well with increasing grain-boundary area of the ceramics except for $Na_{0.68}Ni_{0.34}Ti_{0.66}O_2$. The latter phase exhibits a large amount of glassy phases along the grain boundaries (Fig. 1) due to the high sintering temperature close to melting, which seems to be a reason for higher sensitivity than that of $Na_{0.8}Ni_{0.4}Ti_{0.6}O_2$, despite much larger grains. The maximum and minimum stability in wet atmospheres was found for $Na_{0.68}Ni_{0.34}Ti_{0.66}O_2$ and $Na_{0.8}Fe_{0.8}Ti_{0.2}O_2$ ceramics, respectively.

4. CONCLUSIONS

Sodium cation-conducting ceramics of layered phases $Na_{0.68}Ni_{0.34}Ti_{0.66}O_2$ (P2-type structure), $Na_{0.8}Ni_{0.4}Ti_{0.6}O_2$, $Na_{0.8}Fe_{0.8}Ti_{0.2}O_2$ and $Na_{0.8}Ni_{0.6}Sb_{0.4}O_2$ (O3-type structures) were prepared by the standard solid-state reaction method, $Na_{0.8}Ni_{0.6}Sb_{0.4}O_2$ being synthesized for the first time. The dilatometric studies showed that thermal expansion of Na^+-conducting ceramics is linear at 300-1173 K, with average TEC values varying in the range $(13.7\text{-}16.0)\times10^{-6}$ K^{-1}. A linear correlation between the conductivity of O3-type compounds, predominantly ionic, and thermal expansion coefficients is observed. At temperatures lower than 420 K, increasing vapor partial pressure from approximately 0 (dry air) to 0.46 atm leads to increasing total conductivity of the studied materials, accompanied with water absorption. Impedance spectra suggest that the increase in the conductivity has a dominantly grain-boundary nature; thus, the interaction of studied materials with water vapor is strongly influenced by the ceramic microstructure being favored by large boundary area, porosity and high amount of glassy phase at grain boundaries. $Na_{0.68}Ni_{0.34}Ti_{0.66}O_2$ ceramics exhibit maximum stability in wet atmospheres and also the highest ionic conduction.

ACKNOWLEDGMENTS

This work was supported by the FCT, Portugal (POCTI program and project BD/6594/2001). Helpful discussions with V.B. Nalbandyan, F.M. Figueiredo and J.R. Frade are gratefully acknowledged.

REFERENCES

1. J.M. Paulsen, D. Larcher, J.R. Dahn. "O2 Structure $Li_{2/3}[Ni_{1/3}Mn_{2/3}]O_2$: A New Layered Cathode Material for Rechargeable Lithium Batteries. III. Ion Exchange". J. Electrochem. Soc., **147** [8] 2862-2867 (2000).
2. V. Leonhard, M. Ilgenstein, K. Cammann, J. Krause. "NASICON Electrode for Detecting Sodium-ions". Sensors and Actuators B, **19** [1-3] 329-332 (1994).
3. H. Yagi, T. Saiki. "Humidity Sensor Using NASICON not Containing Phosphorus". Sensors and Actuators B, **5** [1-4] 135-138 (1991).
4. T. Maruyama, S. Sasaki, Y. Saito. "Potentiometric Gas Sensor for Carbon-dioxide Using Solid Electrolytes". Solid State Ionics, **23** [1-2] 107-112 (1987).
5. H. Kohler, H. Schulz. "NASICON Solid Electrolytes. 1. The Na+ Diffusion Path and its Relation to the Structure". Mater. Res. Bull., **20** [12] 1461-1471 (1985).
6. C.R. Peters, M. Bettman, J.W. Moore, M.D. Glick. "Refinement of Structure of Sodium Beta-Alumina". Acta Cryst. B, **27** 1826-1834 (1971).
7. A. Maazaz, C. Delmas, C. Fouassier, J-M. Reau, P. Hagenmuller. "Sur une Nouvelle Famille de Conducteurs Cationiques a Structure Feuilletee de Formule $K_x(L_{x/2}Sn_{1-x/2})O_2$ (L = Mg, Ca, Zn; x<1)". Mater. Res. Bull., **14** 193-199 (1979).
8. M.Y. Avdeev, V.B. Nalbandyan, B.S. Medvedev. "Hexagonal sodium titanate chromite: A new high-conductivity solid electrolyte". Inorg. Mater., **33** [5] 500-503 (1997).
9. V.B. Nalbandyan, I.L. Shukaev. "Ternary sodium nickel oxides". Zh. Neorg. Khim., **37** [11] 2387-2394 (1992) [in Russian].
10. E.I. Burmakin, G.Sh. Shekhtman. "Solid electrolytes in the system Fe_2O_3-TiO_2-Na_2O". Electrokhimiya, **21** [6] 752-757 (1985) [in Russian].
11. Y-L. Shin, M-H. Park, J-H. Kwak, H. Namgoong, O.H. Han. "Ionic Conduction Properties of Layer-Type Oxides $Na_xM_{x/2}^{III}Ti_{1-x/2}^{IV}O_2$ (M = Ni, Co; 0.6≤x≤1.0)". Solid State Ionics **150** 363-372 (2002).
12. Zh. Lu, J.R. Dahn. "Intercalation of Water in P2, T2 and O2 Structure $A_z[Co_xNi_{1/3-x}Mn_{2/3}]O_2$". Chem. Mater., **13** 1252-1257 (2001).
13. J. Rodriguez-Carvajal. "Recent Advances in Magnetic Structure Determination by Neutron Powder Diffraction". Physica B, **192** [1-2] 55-69 (1993).
14. Y-L. Shin, M-Y. Yi. "Preparation and Structural Properties of Layer-Type Oxides $Na_xNi_{x/2}Ti_{1-x/2}O_2$ (0.6≤x≤1.0)". Solid State Ionics, **132** 131-141(2000).
15. V.V. Kharton, A.A. Yaremchenko and E.N. Naumovich. "Research on the electrochemistry of oxygen ion conductors in the former Soviet Union. II. Perovskite-related oxides". J. Solid State Electrochem., **3** [6] 303-326 (1999).
16. V.V. Kharton, E.N. Naumovich, A.A. Yaremchenko and F.M.B. Marques. "Research on the electrochemistry of oxygen ion conductors in the former Soviet Union - IV. Bismuth oxide-based ceramics". J. Solid State Electrochem., **5** [3] 160-187 (2001).
17. V.N. Chebotin. "Physical Chemistry of Solids", p. 99 Khimiya, Moscow (Russia) 1982. [in Russian].
18. A.A. Yaremchenko, V.V. Kharton, E.N. Naumovich and F.M.B. Marques. "Physicochemical and transport properties of bicuvox-based ceramics". J. Electroceramics, **4** [1] 233-242 (2000).
19. V.B. Nalbandyan, L.I. Medvedeva, N.G. Sudorgin, B.S. Medvedev. "Determination of the specific resistivity of ceramic cation-conductors on sodium rare-earth silicates – comparison of methods and identification of error sources". Russ. J. Electrochem., **29** [11] 1207-1214 (1993).
20. Phase Equilibria Diagrams. CD-Rom Database, Ed. P. Schenck, The American Ceramic Society, Westerville, OH, (1998).